Preprint Title	Abrupt elastic to plastic transition in pentagonal nanowires under bending
Authors	Sergei Vlassov, Magnus Mets, Boris Polyakov, Jianjun Bian, Leonid M. Dorogin and Vahur Zadin
Publication Date	21 Aug 2019
Article Type	Full Research Paper
ORCID® iDs	Sergei Vlassov - https://orcid.org/0000-0001-9396-4252

Abrupt elastic to plastic transition in pentagonal nanowires under bending

Sergei Vlassov[1,4*], Magnus Mets[1], Boris Polyakov[2], Jianjun Bian[3], Leonid Dorogin[4], Vahur Zadin[5]

[1] *Institute of Physics, University of Tartu, W. Ostwaldi Str. 1, 50412, Tartu, Estonia*

[2] *Institute of Solid State Physics, University of Latvia, Kengaraga 8, LV-1063, Riga, Latvia*

[3] *Department of Industrial Engineering, University of Padova, Via Gradenigo 6/a, 35131 Padova, Italy*

[4] *ITMO University, Kronverskiy pr., 49, 197101 Saint-Petersburg, Russia*

[5] *Institute of Technology, University of Tartu, Nooruse 1, 50411 Tartu, Estonia*

∗Corresponding author. Tel.: +37255941841

E-mail address: sergei.vlassov@ut.ee (S. Vlassov)

Abstract

In this study, pentagonal Ag and Au nanowires (NWs) were bent in cantilever beam configuration inside a scanning electron microscope. We demonstrated unusual abrupt elastic-to-plastic transition, observed as sudden change of the NW profile from smooth arc-shaped to angled knee-like during the bending in the narrow range of bending angles. In contrast to behavior of NW in tensile and three-point bending test, where extensive elastic deformation was followed by brittle fracture, in our case after the abrupt plastic event NW was still far from fracture and enabled further bending without breaking. Moreover, we found that if NWs are coated with alumina, abrupt plastic event is not observed and NWs can withstand severe deformation in elastic regime without fracture. Mechanical durability under high and inhomogeneous strain fields is an important aspect of exploiting of Ag and

Au NWs in applications like waveguiding or conductive network in flexible polymer composite materials.

Introduction

Nanostructures of noble metals with face centered cubic (FCC) crystal structure (Au, Ag and Cu according to common physical definition) prepared via soft-chemical colloidal techniques often demonstrate morphologies with axes of fivefold (pentagonal) symmetry [1]. Depending on the synthesis conditions such structures can be synthesised in the form of 0D nanoparticles or high-aspect ratio 1D nanowires (NWs) with pentagonal cross-section [2,3]. Structure of pentagonal NWs can be considered as 1D material consisting from five prismatic monocrystalline domains with triangular cross-section rotated relative to each other by approx. 72° as shown schematically in Figure 1. Crystalline domains are divided by twin boundaries [4,5]. Due to the fact that the five triangles cannot make 360◦, such exotic structure cannot exist without internal strains with corresponding mechanical stresses and stored elastic energy proportional to the volume [6].

Inner stresses and peculiar structure of pentagonal materials is expected to lead to mechanical properties different from those of regular monocrystals [7]. This fact must be taken into account when considering applications in which nanocrystals are subjected to mechanical deformation, like e.g. NW-based nanoswitches [8], nanoresonators [9] and flexible electronics [10,11] In the last case NWs are used as a conductive network in composition with flexible polymer materials like e.g. polydimethylsiloxane (PDMS) [12,13]. Reliability of flexible devices in high-strain conditions will be governed by mechanical reliability of individual NWs inside the conductive network [14–16]. Ag NWs are a promising material for flexible transparent electrodes [17]. Plasmon propagation and the optical properties of Ag and Au NWs made them attractive for nanophotonics as waveguides for visible light [18–23]. In all these applications NWs may experience severe and sometimes repeated bending deformations. Therefore, proper understanding of the mechanical behaviour of NWs under bending

deformation and the use of appropriate theoretical models is essential for designing and functioning of NW-based devices.

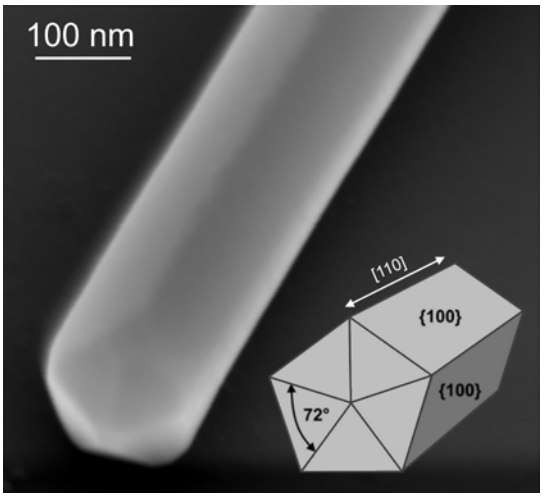

Figure 1. Schematics and SEM image of pentagonal silver nanowire (Ag NW). SEM image reproduced from [28]; Copyright © 2013 Elsevier B.V.

Mechanical properties of pentagonal NWs were studied both theoretically and experimentally in different configurations including uniaxial loading (tensile and compression tests) [24,25], three-point bending [26,27], cantilever beam bending [28,29] and nanoindentation [30]. Several interesting phenomena were reported that can be attributed to peculiar inner structure of pentagonal NWs. Qin et al reported on recoverable plasticity in penta-twinned Ag NWs [31] in tensile test. Enhanced elasticity, exceptional strength and unexpected brittle failure of pentagonal Ag NWs were reported by Zhu et al [25] in tensile test and by Wu et al [27] in three-point bending test. According to authors, grain orientation and grain-boundary organization within these wires was responsible for their anomalous strength and brittle failure. Namely, slip directions in the grains intersect with the twinning boundaries that extend along the entire wire length resulting in uniformly hardened structure. Consequently, the fivefold grain boundaries in these wires intersect with all possible slip systems and so the motion of dislocations associated with the initiation of plastic deformation along any slip direction is restricted by the twinning boundaries that extend into the center of the wire. In this manner, the fivefold twinned silver NWs are effectively grainboundary hardened materials, which sacrifices ductility for strength.

Because the twin boundaries exist along the entire length of wire, the whole wire is uniformly hardened and there are no defects that limit the strength of the wire [27].

In both tensile and three-point bending tests NW is rigidly fixed from both ends. Even though NW is bent in three-point bending test, the deflection of NW before failure is relatively small in comparison to so called pure bending conditions when one of the NW ends is free. From the viewpoint of applications like e.g. waveguiding, behavior of NW under pure bending condition, as opposed to tensile or three-point bending, is of the great importance, as it is related to the ability of NWs to form curved pathways for electro-magnet radiation. Any crack or other discontinuities that can be introduced by bending can prevent plasmon propagation in the NW [19].

Pure bending conditions are realized in cantilever beam bending configuration where NW is fixed from one end and the free end is pushed by the probe. Such configuration enables to perform high degrees of bending. Behavior of Ag NWs under pure bending conditions was studied experimentally by Vlassov et. al in cantilever beam bending test. Similar to Zhu and Wu, we noticed brittle-like fracture of NWs in 1/3 of cases. In 2/3 of cases plastic yield was reported. However, it should be noted, that loading was applied in dynamic mode i.e. the probe was oscillating at frequency around 32 KHz and the amplitude of the oscillations was comparable to the diameter of NWs. Therefore, it is difficult to exclude the possible fatigue effect indicating the need of performing cantilever beam bending test at continuous loading mode.

In present work we performed bending tests of pentagonal Ag and Au NWs in cantilever beam configuration inside a scanning electron microscope (SEM) for visual guidance. We demonstrate unusual abrupt elastic-to-plastic transition, observed as sudden change of the NW profile from smooth arc-shaped to angled knee-like during the bending in the narrow range of bending angles (*critical bending angle*). Moreover, we show that if NWs are coated with alumina, abrupt plastic event is not observed and NWs can withstand severe deformation in elastic regime without fracture.

Materials and methods

Nanowires: Ag NWs were purchased from Blue Nano (USA). Au NWs were purchased from Smart Materials (Latvia) [32].

SEM and TEM characterization. Micrographs of NWs were obtained with high-resolution scanning electron microscope (HR-SEM, Helios Nanolab 600, *FEI*) and TEM (Tecnai GF20, FEI). NWs were drop-casted on either TEM grids with lacey carbon (Agar, UK) for TEM characterization, or on glassy carbon and silicon wafers (100, n/phosphorus doped, 3-6 ohm·cm, *Mat-Technology*) for SEM imaging.

Experimental set-up for bending test: NWs were drop-casted on TEM grid (Agar) so that some NWs were partly suspended over a hole. Bending test were performed inside a HR-SEM with a cantilever beam-bending configuration. NWs were bent in plane with a substrate by an AFM probe (ATEC−CONT cantilevers, Nanosensor, Neuchatel, Switzerland, C = 0.2 N m−1) attached to a micromanipulator (MM3AEM, Kleindiek, Germany).

FEM Simulations: The cantilevered beam bending experiments were simulated using FEM COMSOL Multiphysics 5.2 solid mechanics module. For this the linear elastic material model from COMSOL was chosen. Simulations were based on a recently developed segmented pentagonal NW model [29] In this model, the pentagonal NW was composed of five triangular prism-shaped domains with vertex angle of 72°. These domains represent the FCC monocrystallites. Each domain was assigned an elasticity matrix of Ag or Au corresponding to their crystal structure to account for structural anisotropy. The elasticity matrix independent parameters in Voigt notation for Ag were C_{11}=124 GPa, C_{12}=93.4 GPa, C_{44}=46.1 GPa and for Au C_{11}=190 GPa, C_{12}=161 GPa, C_{44}=42.3 GPa. The NW was fixed by a portion of the bottom facet at one end and pushed at the other end by applying gradually increasing force. The mesh used in these simulations is described in previous work [29].

The yield strength values were obtained from the FEM NW model by fitting its profile to the experimentally bent profiles of Ag or Au NWs at the critical bending angle, before the abrupt transition to plastic deformation.

MD simulations: Classical molecular dynamics (MD) simulations are conducted to investigate the atomic deformation behaviour of the penta-twinned Ag NW under bending. The large-scale open-source molecular dynamics simulator, LAMMPS, developed by Sandia National Laboratories, is adopted [33]. The interatomic interactions are described by the widely used embedded atom method (EAM), and a potential for Ag is utilized here [34]. Due to the limitation of computational resources, the size of the nanowire in simulation is much smaller than that in experiments. Figure 2a shows the atomic configuration of the penta-twinned NW in present simulation. The simulated model is ~ 60.0 nm in length and ~ 14.2 nm in diameter. The total number of the Ag atoms is ~ 0.474 million. Fig. 1b shows the initial five-fold internal twin structures. In simulation, free boundary conditions are imposed in all directions. The time evolutions of atoms are within the framework of canonical (NVT) ensemble, and the time step is chosen as 2.0 fs. The Nosé-Hoover thermostat is used to adjust the temperature of the atomic system around 300 K [35,36].

After construction of the NW, structural relaxation is firstly performed by using conjugated gradient method in order to make the configuration reach a local stable state. The NW is further equilibrated at 300 K for about 40 ps to relax the internal stress. Fig. 1c shows the distribution of von Mises stress on the cross-section after this equilibration. To perform bending load to the NW, at the fixed end, atoms with a layer thickness of 4 nm (the part colored in red in Figure 2a) are kept and fixed in perfect lattice. At the free end, atoms with a layer thickness of 1.0 nm (the part colored in yellow in Figure 2) are kept rigid, and will move as a whole. The rigid layer is then coupled to a spring with stiffness of 30.0 N/m. In the loading procedure, the free end of the spring moves at a constant speed of 0.05 Å/ps, and the NW will be bent by the spring. We monitor the bending force exerted by the spring to the NW and the displacement of the rigid free end to characterize the loading response of the NW.

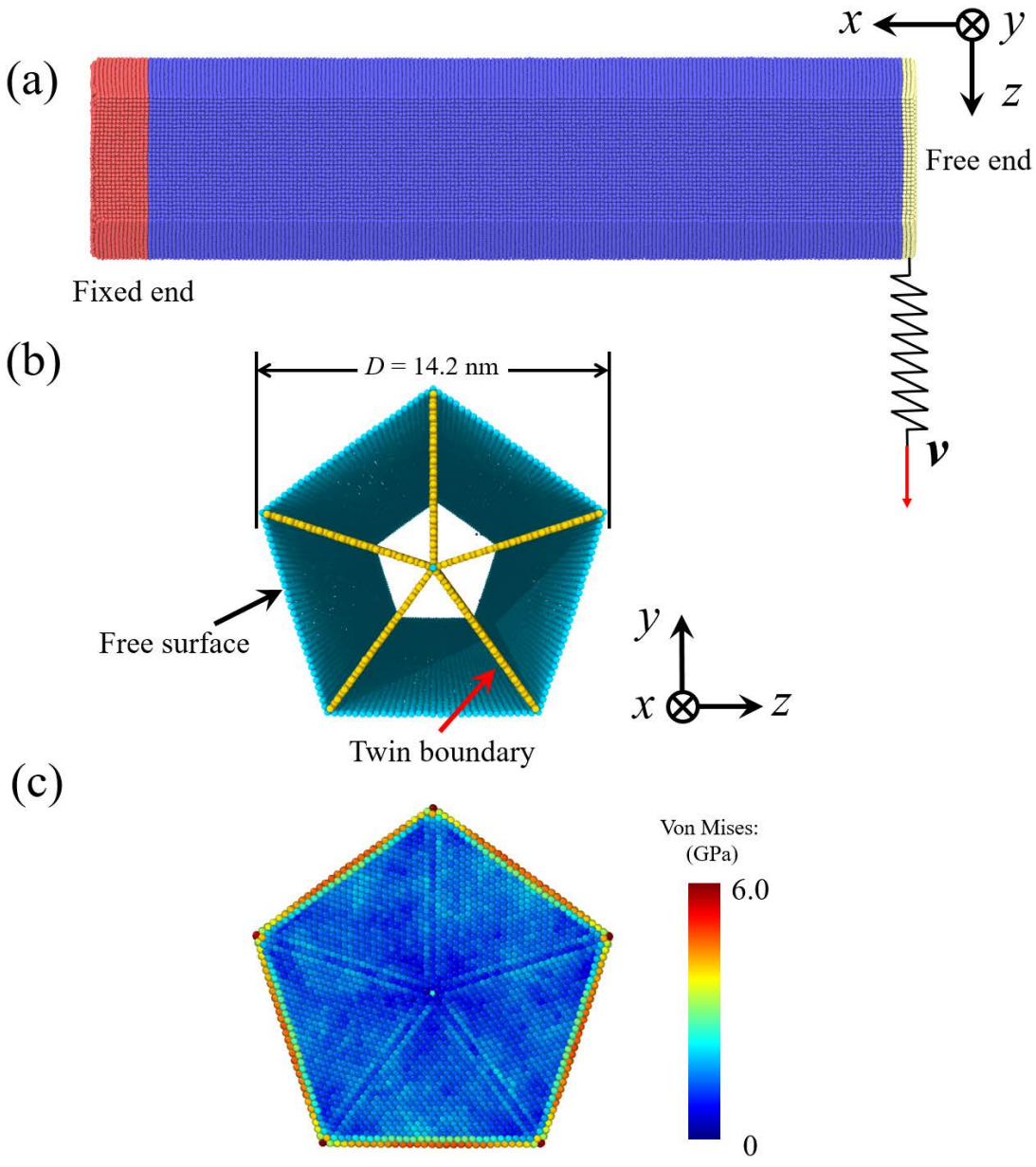

Figure 2. (a) Atomic simulation model of the Ag NW, (b) the internal twin structures (atoms in perfect lattice and those at the two ends are not shown for clearness), and (c) the distribution of von Mises stress on the cross section.

Results and discussion

According to SEM and TEM images both Ag and Au NWs had uniform diameters with pentagonal cross-section and well pronounced facets. Diameters ranged from several tens of nm to over 100 nm with length ranging from several hundred nm to tens of micrometers. Some NWs had clearly pronounced angled profile, that resembled some sort of a so-called “greenstick fracture” (Figure 3). Visually very similar phenomena was reported for Ag NWs by Peng et al [37] and explained as joining of two adjacent NWs. In present work we challenged the explanation given by Peng et al and performed in-situ SEM bending and breaking of Ag in order to find if the visible profile of NWs is related to brittle-like mechanical deformation rather that joining of two NWs together. Experiments were also performed on Au NWs to find if the observed phenomena is material dependent or rather related to inner five-fold twinned structure.

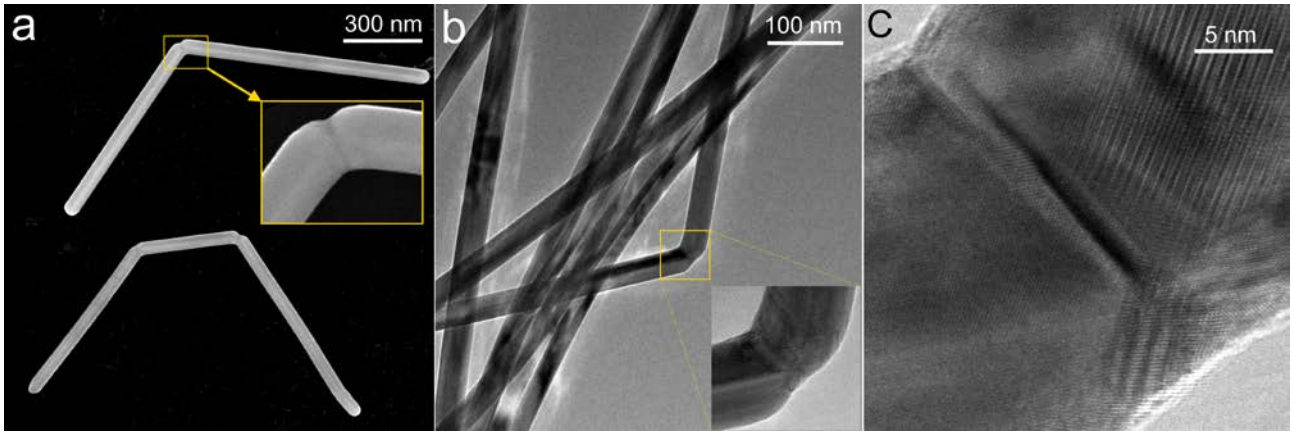

Figure 3. SEM (a) and TEM (b,c) images of deformed Ag NWs drop-casted from a solution.

When either Ag or Au NWs were gradually bent by a sharp Si tip in a cantilever beam configuration inside SEM, abrupt elastic-to-plastic transition event was revealed at a *critical bending angle*. Namely, in the beginning of the bending test NWs exhibited extensive elastic behavior, common for one-dimensional nanostructures [38]. However, at certain curvature bending profile of NW suddenly underwent from smooth arc-shaped to angled knee-like bend (Figure 4). This behavior was general for both Ag and Au NWs. This finding was not trivial, since macroscopic Ag and Au undergoes

gradual plastic deformation under loading. In our case NWs underwent an abrupt event of plastic deformation to a new crystallographic configuration. This new configuration was elastically stable, i.e. if "angled" NW was moderately bent by AFM tip either further or straightened and then released, it went back to its initial angled profile. Moreover, a complete fracture was difficult to achieve in such configuration even at severe deformations.

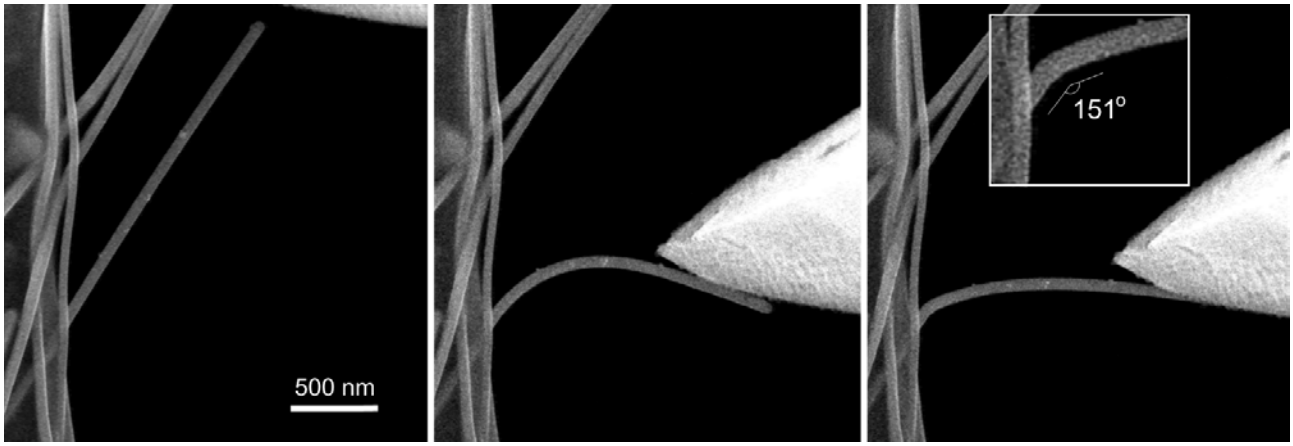

Figure 4. Ag NW bending experiment observed inside a SEM. (a) straight NW before bending, (b) NW bent close to the critical bending angle, (c) abrupt elastic-to-plastic transition occurred.

In total 19 (6 Ag and 13 Au) NWs were tested and it was found that the angle of the deformed NWs after initial plastic event lies in the narrow range of angles (151 – 169 degrees) for both Ag and Au with median value of 163 ± 5.6 degrees (Figure 5). This fact indicates that observed abrupt elastic-to-plastic transition is not random process but is tightly related to inner structure of the five-fold twinned NWs.

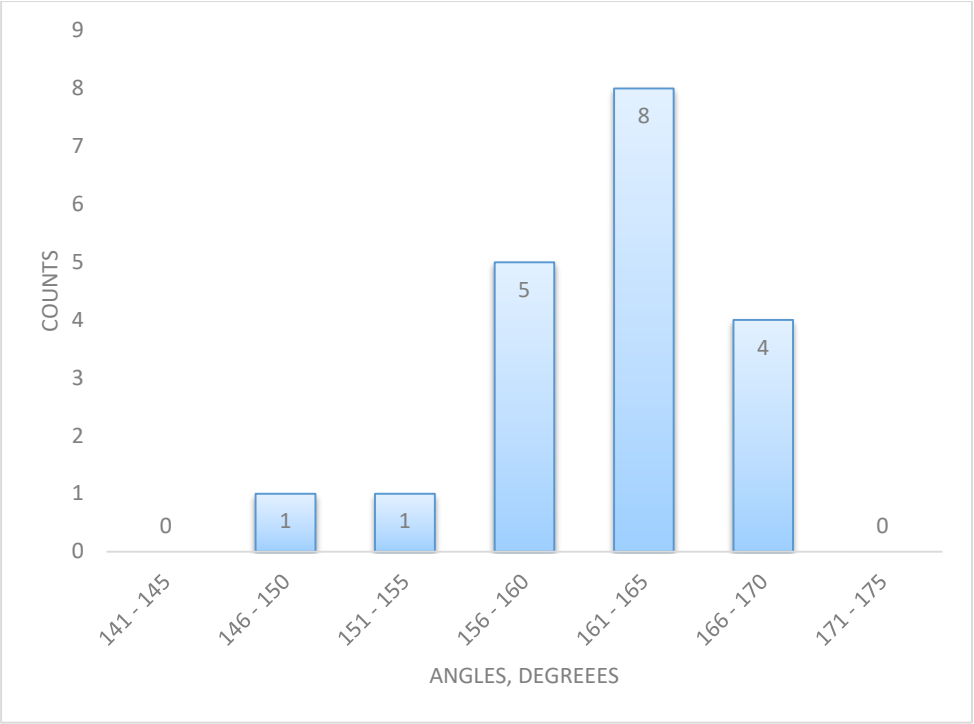

Figure 5. Distribution of angles of the deformed NWs after abrupt plastic event in the bending tests.

In order to obtain yield strength values and to have more clear understanding regarding stresses present in the NW during yielding FEM model was developed that included inner anisotropy of fivefold twinned NW. Geometrical parameters and maximal deformation of the NWs at the *critical bending angle* (prior transition) were taken from the real experiments.

The Von Mises stress distribution for FEM-simulated bent NW is shown in Figure 5. The stresses are concentrated mostly on two edges of the bent NW near the fixed part. The highest stress values are on the outer edge in the range from 4.65 GPa to 6.54 GPa for Ag NWs and from 5.1 GPa to 9.4 GPa for Au NWs (Figure 7). Median yield strength values for Ag and Au NWs are 5.6 GPa and 6.8 GPa, respectively. Tendency for increasing the strength at smaller diameters (size effect) can be noticed.

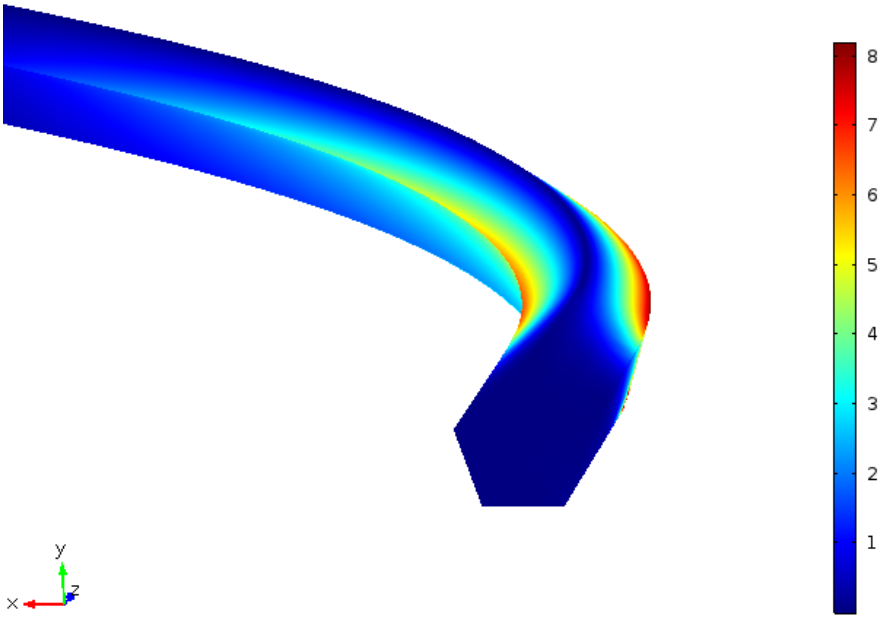

Figure 6. Von Mises stress distribution in bent Au NW at the critical bending angle, corresponding to maximal experimental curvature prior to fracture (GPa).

For Ag NWs, the results are in good accordance with experimental yield strength values obtained for Ag NWs using the similar mechanical characterization method [28]. To our knowledge, no experimental works determining the strength of pentagonal Au NWs have not been published yet, therefore direct comparison cannot be made. Nonetheless, the values obtained in the present work are comparable, but not exceeding the theoretical yield strength value of bulk Au, which is about 8 GPa in accordance with empirical relation E/10 based on atomic bonding considerations [39].

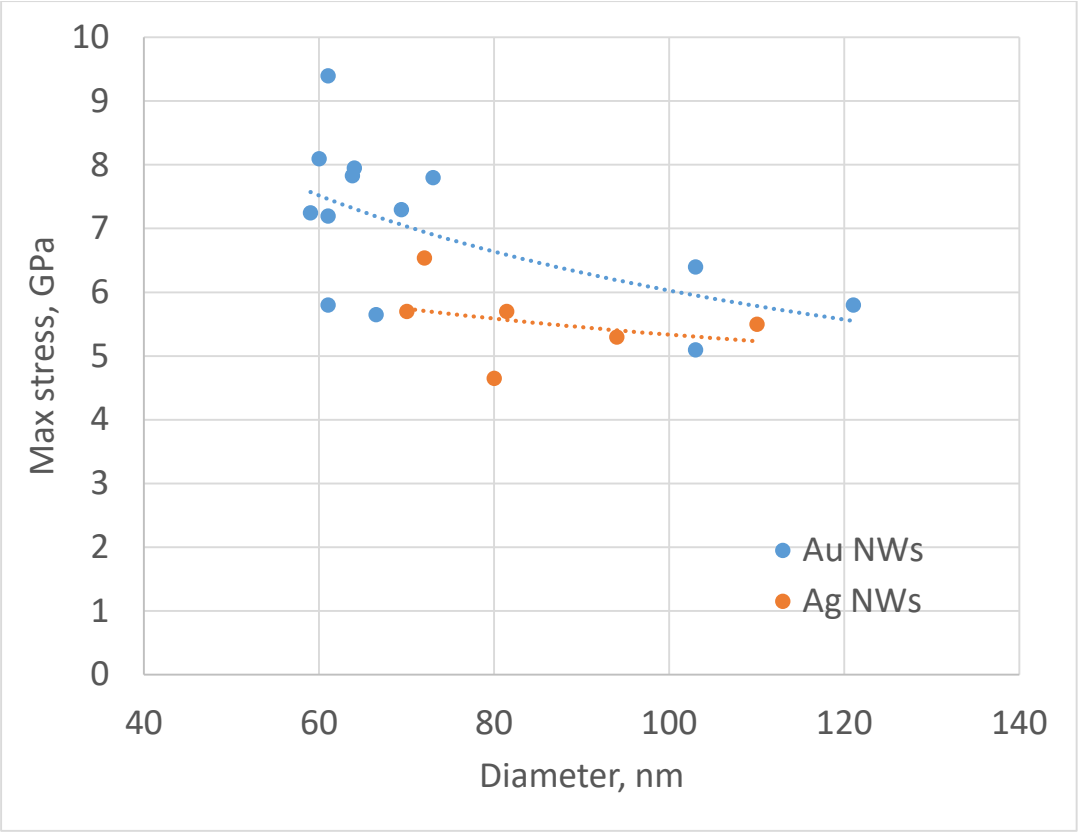

Figure 7. Au and Ag NWs yield strengths as revealed from the bending tests.

Results (MD)

Figure 8 depicts the loading curve of the penta-twinned NW. Owing to the influences of temperature and the natural frequencies of the atomic system, NW vibrates during the loading procedure, leading to the oscillation of bending load. When referring to the loading curve, we only consider the whole trend. In the elastic regime, the loading force linearly increases with the displacement. When yielding occurs, load drops abruptly. We examine the atomistic structure of the NW immediately after the load peak. The bending angle of the NW at the abrupt elastic-to-plastic transition is ~ 164°, which agrees very well with transition angles 163 ± 5.6 degrees observed in experiment. Dislocations nucleate from free surface as marked by the white circles (Panel i of Figure 8). After nucleation, partial dislocations glide toward the core region of the NW, and experience the impediment from the existing twin boundaries [40]. With the progressing of bending deformation, another dislocation source is also activated, and new dislocation nucleation and propagation lead to the second distinct load drop of the

loading curve (Panel ii of Figure 8). In following stage, the bending force gradually becomes stable around 15 nN, and dislocations continue to nucleate in the region close to the fixed end. Besides the existing twin boundaries, deformation twin could also be observed (Panel iii of Figure 8). Interaction of continuously nucleated dislocation will form an amorphous layer, similar to grain boundary. With the concentration of the deformation, surface necking occurs which will lead to the ductile fracture of the NW. Upon unloading, some dislocations may retract and annihilate at free surface, which is promoted by the existing twin boundaries [31], and the amorphous atomic layer and surface necking remain (Panel iv of Figure 8).

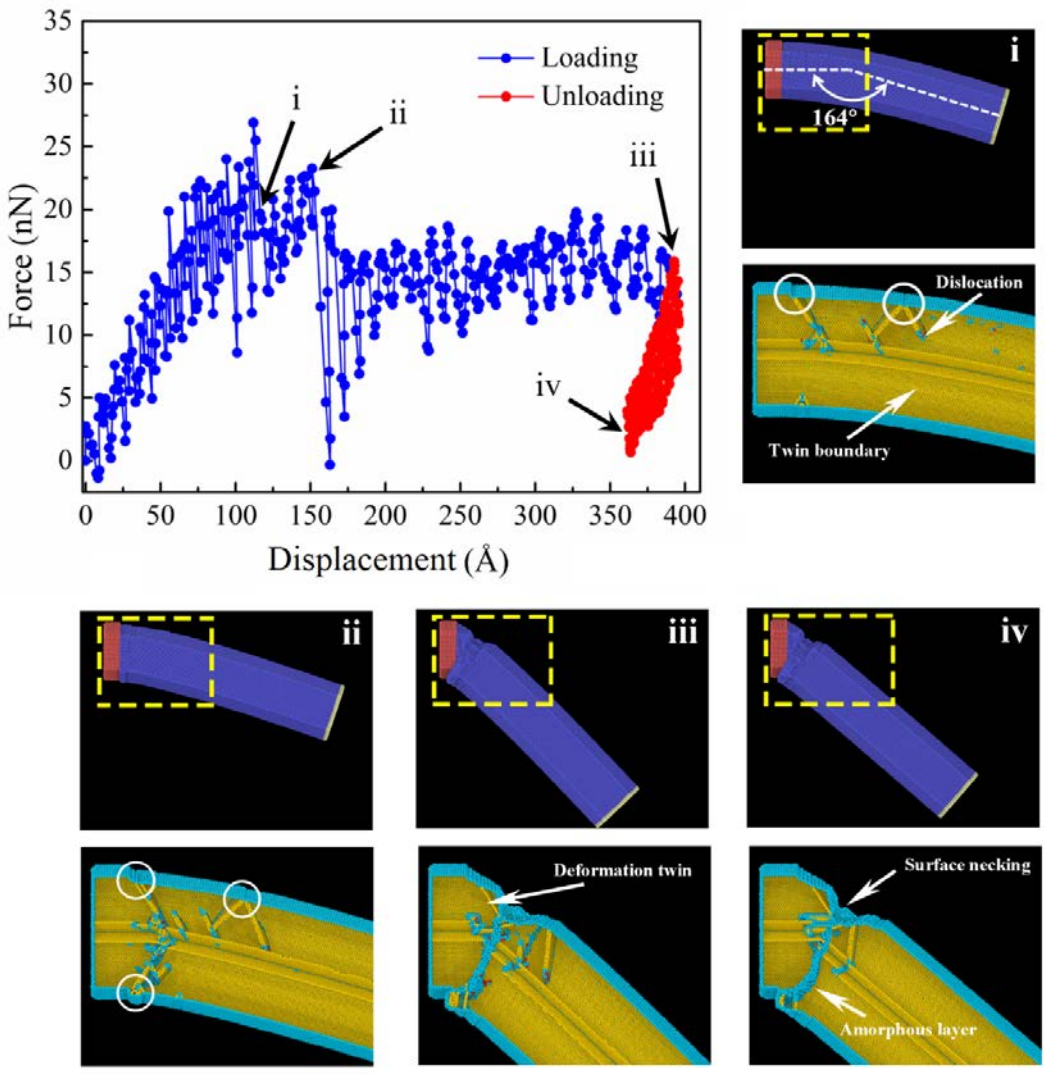

Figure 8. Bending force versus displacement curve (Top) and the evolution of the atomic structure and the internal defects during bending of the NW (Bottom). In the local cross-section of the NW, atoms in perfect lattice are not shown for clearness.

On the basis of conducted experiments, electron microscopy observations and numerical simulations we can speculate about possible reasons behind observed phenomena. The abrupt elastic to plastic deformation transition of the FCC pentagonal NWs under cantilevered beam bending can be attributed to their inner structure. The plastic deformation in metals is the result of formation and propagation of dislocation defects. For the pentagonal NWs, the propagation of these defects is hindered by the five twin boundaries inside these structures leading to the accumulation of dislocations at the twin boundaries [41]. In the cantilevered beam bending configuration this accumulation is more pronounced due to asymmetric deformation. This dislocation pile up can result in increased strength and may lead to sudden stress release, which is observed as abrupt plastic event.

Surface nucleation of dislocation in nanoscale objects such as NWs might play a major role in plastic yield due to their extreme surface-to-volume ratio. If surface nucleation is mitigated by, e.g. external materials (coating), the onset of plastic yield can be significantly postponed. Hence, we performed few preliminary tests on Ag NWs coated by ALD with few-nm thick layer of alumina (Figure 7). Abrupt elastic-to-plastic transition was not observed even for bending curvatures up to 90 degrees. Hard coating may prevent stress release mechanisms related to dislocation pile up and dislocation nucleation at the surface [42,43]. However, more systematic studies on the role of coating need to be conducted and this will be addressed in our future research.

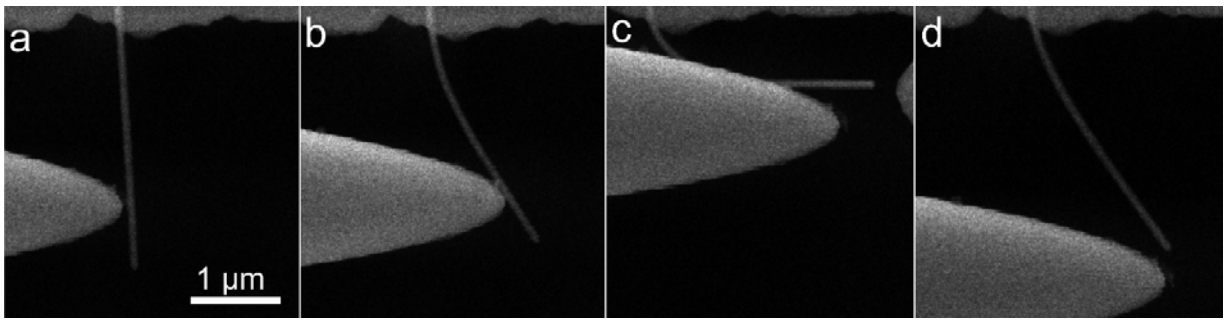

Figure 9. Bending of alumina-coated silver NW. No breaking or abrupt deformation were observed even for relatively high bending curvatures.

Conclusion

We demonstrated abrupt elastic-to-plastic transition event for Ag and Au NWs in cantilever beam bending test inside SEM. Event consisted in abrupt transition from arc-shaped profile to angled profile in the narrow range of angles: 163 ± 5.6 degrees measured on 19 NWs. Maximal stress values in the most bent state prior transition were 5.6 GPa and 6.8 GPa for Ag and Au NWs respectively, which is close to the theoretical strength of this materials. The abrupt transition can be attributed to the two factors: the inner structure of the pentagonal NWs, and its free surface. The five twin boundaries dividing the structure can hinder the propagation of dislocations and prevents a smooth onset of plastic deformation under cantilevered beam bending configuration. Therefore, the accumulation of dislocations at the twin boundaries leads to the brittle fracture-like onset of plastic deformation. The free surface of NW facilitates nucleation of defects, such as dislocations in otherwise practically defect-free pentagonal NW structure. Additional preliminary experiments with alumina-coated Ag NWs showed that coating can increase bending strength of the NWs.

Acknowledgement

MD modeling and calculations were supported by Russian Science Foundation project grant 18-19-00645 "Adhesion of polymer-based soft materials: from liquid to solid"; mechanical testing and FEM simulations were supported by Estonian Research Council projects PUT1689 and PUT1372 respectively.

References

[1] J. L. Elechiguerra, J. Reyes-Gasga, M. J. Yacaman, *J. Mater. Chem.* **2006**, *16*, 3906.
[2] Y. Sun, Y. Xia, *Adv. Mater.* **2002**, *14*, 833.
[3] J. Reyes-Gasga, J. L. Elechiguerra, C. Liu, A. Camacho-Bragado, J. M. Montejano-Carrizales, M. Jose Yacaman, *J. Cryst. Growth* **2006**, *286*, 162.

[4] H. Chen, Y. Gao, H. Zhang, L. Liu, H. Yu, H. Tian, S. Xie, J. Li, *J. Phys. Chem. B* **2004**, *108*, 12038.
[5] V. G. Gryaznov, J. Heydenreich, A. M. Kaprelov, S. A. Nepijko, A. E. Romanov, J. Urban, *Cryst. Res. Technol.* **1999**, *34*, 1091.
[6] L. M. Dorogin, S. Vlassov, A. L. Kolesnikova, I. Kink, R. Lõhmus, A. E. Romanov, *Phys. Status Solidi B* **2010**, *247*, 288.
[7] J. Y. Wu, S. Nagao, J. Y. He, Z. L. Zhang, *Nano Lett.* **2011**, *11*, 5264.
[8] O. Y. Loh, H. D. Espinosa, *Nat. Nanotechnol.* **2012**, *7*, 283.
[9] M. Li, R. B. Bhiladvala, T. J. Morrow, J. A. Sioss, K.-K. Lew, J. M. Redwing, C. D. Keating, T. S. Mayer, *Nat. Nanotechnol.* **2008**, *3*, 88.
[10] R. Zhang, M. Engholm, *Nanomaterials* **2018**, *8*, 628.
[11] Y. Shi, L. He, Q. Deng, Q. Liu, L. Li, W. Wang, Z. Xin, R. Liu, *Micromachines* **2019**, *10*, 330.
[12] F. Xu, Y. Zhu, *Adv. Mater.* **2012**, *24*, 5117.
[13] M. Amjadi, A. Pichitpajongkit, S. Lee, S. Ryu, I. Park, *ACS Nano* **2014**, *8*, 5154.
[14] G.-W. Huang, H.-M. Xiao, S.-Y. Fu, *Sci. Rep.* **2015**, *5*, 13971.
[15] C.-J. Lee, K. H. Park, C. J. Han, M. S. Oh, B. You, Y.-S. Kim, J.-W. Kim, *Sci. Rep.* **2017**, *7*, 1.
[16] R. Helgason, A. Banavali, Y. Lai, *Med. DEVICES Sens.* **2019**, *2*, e10025.
[17] J.-Y. Lee, S. T. Connor, Y. Cui, P. Peumans, *Nano Lett.* **2008**, *8*, 689.
[18] P. r. West, S. Ishii, G. v. Naik, N. k. Emani, V. m. Shalaev, A. Boltasseva, *Laser Photonics Rev.* **2010**, *4*, 795.
[19] W. Wang, Q. Yang, F. Fan, H. Xu, Z. L. Wang, *Nano Lett.* **2011**, *11*, 1603.
[20] Y. Wang, X. Guo, L. Tong, J. Lou, *J. Light. Technol.* **2014**, *32*, 3631.
[21] H. Wei, H. Xu, *Nanophotonics* **2012**, *1*, 155.
[22] G. Kartopu, K.-L. Choy, O. Yalçın, *Phys. Scr.* **2014**, *89*, 095801.
[23] S. Nauert, A. Paul, Y.-R. Zhen, D. Solis, L. Vigderman, W.-S. Chang, E. R. Zubarev, P. Nordlander, S. Link, *ACS Nano* **2014**, *8*, 572.
[24] F. Niekiel, E. Spiecker, E. Bitzek, *J. Mech. Phys. Solids* **2015**, *84*, 358.
[25] Y. Zhu, Q. Qin, F. Xu, F. Fan, Y. Ding, T. Zhang, B. J. Wiley, Z. L. Wang, *Phys. Rev. B* **2012**, *85*, DOI 10.1103/PhysRevB.85.045443.
[26] G. Y. Jing, H. L. Duan, X. M. Sun, Z. S. Zhang, J. Xu, Y. D. Li, J. X. Wang, D. P. Yu, *Phys. Rev. B* **2006**, *73*, DOI 10.1103/PhysRevB.73.235409.
[27] B. Wu, A. Heidelberg, J. J. Boland, J. E. Sader, Sun, Li, *Nano Lett.* **2006**, *6*, 468.
[28] S. Vlassov, B. Polyakov, L. M. Dorogin, M. Antsov, M. Mets, M. Umalas, R. Saar, R. Lõhmus, I. Kink, *Mater. Chem. Phys.* **2014**, *143*, 1026.
[29] M. Mets, M. Antsov, V. Zadin, L. M. Dorogin, A. Aabloo, B. Polyakov, R. Lõhmus, S. Vlassov, *Phys. Scr.* **2016**, *91*, 115701.
[30] M. Lucas, A. M. Leach, M. T. McDowell, S. E. Hunyadi, K. Gall, C. J. Murphy, E. Riedo, *Phys. Rev. B* **2008**, *77*, DOI 10.1103/PhysRevB.77.245420.
[31] Q. Qin, S. Yin, G. Cheng, X. Li, T.-H. Chang, G. Richter, Y. Zhu, H. Gao, *Nat. Commun.* **2015**, *6*, 5983.
[32] F. Kim, K. Sohn, J. Wu, J. Huang, *J. Am. Chem. Soc.* **2008**, *130*, 14442.
[33] S. Plimpton, *J. Comput. Phys.* **1995**, *117*, 1.
[34] P. L. Williams, Y. Mishin, J. C. Hamilton, *Model. Simul. Mater. Sci. Eng.* **2006**, *14*, 817.
[35] S. Nosé, *J. Chem. Phys.* **1984**, *81*, 511.
[36] W. G. Hoover, *Phys. Rev. A* **1985**, *31*, 1695.
[37] P. Peng, L. Liu, A. P. Gerlich, A. Hu, Y. N. Zhou, *Part. Part. Syst. Charact.* **2013**, *30*, 420.
[38] B. Polyakov, L. M. Dorogin, S. Vlassov, M. Antsov, P. Kulis, I. Kink, R. Lohmus, *Eur. Phys. J. B* **2012**, *85*, DOI 10.1140/epjb/e2012-30430-6.
[39] M. R. Falvo, R. M. Taylor Ii, A. Helser, V. Chi, F. P. Brooks Jr, S. Washburn, R. Superfine, *Nature* **1999**, *397*, 236.
[40] S. Narayanan, G. Cheng, Z. Zeng, Y. Zhu, T. Zhu, *Nano Lett.* **2015**, *15*, 4037.

[41] A. M. Leach, M. McDowell, K. Gall, *Adv. Funct. Mater.* **2007**, *17*, 43.
[42] S. Vlassov, B. Polyakov, L. M. Dorogin, M. Vahtrus, M. Mets, M. Antsov, R. Saar, A. E. Romanov, A. Lõhmus, R. Lõhmus, *Nano Lett.* **2014**, *14*, 5201.
[43] S. Vlassov, B. Polyakov, M. Vahtrus, M. Mets, M. Antsov, S. Oras, A. Tarre, T. Arroval, R. Lõhmus, J. Aarik, *Nanotechnology* **2017**, *28*, 505707.
[44] F. F. Csikor, C. Motz, D. Weygand, M. Zaiser, S. Zapperi, *Science* **2007**, *318*, 251.